

Article

Monitoring the Geopolymerization Reaction of Geopolymer Foams Using ^{29}Si and ^{27}Al MAS NMR

Ghizlane Moutaoukil ^{1,2}, Isabel Sobrados ^{2,*} , Saliha Alehyen ¹ and M'hamed Taibi ¹

¹ Laboratoire de Physico-Chimie des Matériaux Inorganiques et Organiques (LPCMIO), Centre des Sciences des Matériaux, Mohammed V University (UM5), Ecole Normale Supérieure (E.N.S), Rabat BP 5118, Morocco; ghizlane.moutaoukil9@gmail.com (G.M.); alehyensali@yahoo.fr (S.A.); taibiens@yahoo.fr (M.T.)

² Instituto de Ciencia de Materiales de Madrid, Consejo Superior de Investigaciones Científicas (CSIC), C/Sor Juana Inés de la Cruz, 3, ES, 28049 Madrid, Spain

* Correspondence: isobrado@icmm.csic.es

Abstract: This study aims to investigate the geopolymerization reaction of geopolymer foams produced with three different foaming agents: aluminum powder, zinc powder, and hydrogen peroxide. The geopolymerization reaction of geopolymer foam was monitored using the ^{27}Al and ^{29}Si magic angle spinning (MAS) nuclear magnetic resonance (NMR) spectroscopy technique. ^{27}Al MAS-NMR was used to monitor the reaction at an early stage, while ^{29}Si and ^{27}Al MAS-NMR analyses were employed at specific time intervals of 3, 6, 10, 15, and 28 days to examine the changes that occurred in the formed gel over time. We discussed in detail how the type of foaming agent used and the duration of the reaction both influence the quantity of gel formed and the amount of remnant fly ash. Our findings indicate that the type of foaming agent used affects the formation and structure of the gel, with aluminum powder leading to the highest gel formation. Additionally, the duration of the reaction plays a significant role in determining the quantity of remnant fly ash, with longer reaction times resulting in decreased fly ash content. This study sheds light on the relevance of understanding the role of foaming agents in the geopolymerization reactions of geopolymer foams and the influence of reaction time on the formed gel properties.

Keywords: geopolymer foam; ^{29}Si and ^{27}Al MAS NMR; foaming agent; geopolymerization reaction



Citation: Moutaoukil, G.; Sobrados, I.; Alehyen, S.; Taibi, M. Monitoring the Geopolymerization Reaction of Geopolymer Foams Using ^{29}Si and ^{27}Al MAS NMR. *Minerals* **2024**, *14*, 516. <https://doi.org/10.3390/min14050516>

Academic Editor: Elsabe Kearsley

Received: 13 April 2024

Revised: 6 May 2024

Accepted: 12 May 2024

Published: 16 May 2024



Copyright: © 2024 by the authors. Licensee MDPI, Basel, Switzerland. This article is an open access article distributed under the terms and conditions of the Creative Commons Attribution (CC BY) license (<https://creativecommons.org/licenses/by/4.0/>).

1. Introduction

Alkaline activation of aluminosilicates leads to polymerization of silicon, oxygen, and aluminum species to form an inorganic material with an amorphous three-dimensional framework called a geopolymer [1,2]. The structural units of geopolymers consist of tetrahedrally coordinated aluminum and silicon atoms linked to bridging (BO) and non-bridging (NBO) oxygen atoms [3–5]. Magic angle spinning nuclear magnetic resonance (MAS-NMR) is a powerful tool for studying the structure of silicates [5,6] and aluminosilicates [7,8], including geopolymers [9,10]. This technique provides detailed information on the coordination of aluminum and silicon atoms with bridging and non-bridging oxygen atoms, which is critical in understanding the formation process of these materials [11–13]. Additionally, MAS-NMR can be used to determine the chemical shifts, coupling constants, and quadrupolar interaction parameters, which provide further insight into the structure and bonding of the material. The results obtained from MAS-NMR can be compared with other characterization techniques such as X-ray diffraction and infrared spectroscopy to obtain a comprehensive understanding of geopolymers' structure and properties [14,15].

Aluminum is an ideal nucleus for NMR spectroscopy due to its natural abundance of 100% and fast relaxation times [12]. This means that NMR spectra can be acquired with good quality in relatively short measurement times, which is a desirable feature in NMR spectroscopy [16]. The ^{27}Al spin of $I = 5/2$ results in a nuclear quadrupolar

moment, which can interact with the electric field gradients that surround the nucleus [17]. This interaction results in characteristic peaks in the NMR spectrum that can be used to determine the structure of a molecule and other important information about the sample being studied. Overall, the combination of ^{27}Al 's natural abundance, fast relaxation times, and quadrupolar moment makes it a valuable tool for NMR spectroscopy.

^{29}Si has a spin $I = 1/2$, implying that it is not susceptible to quadrupole peak broadening and distortion. Although its natural abundance is relatively low (4.7%), the spectral resolution of ^{29}Si is high because of its relatively narrow resonance lines [6,12,17].

The nearest neighbor modifications generate smaller but measurable variations in the chemical shift of ^{29}Si in the range of 10 ppm as the connectivity changes from Q2 to Q3 to Q4 units [12,18]. When the next closest neighboring element is changed, a similar magnitude of change is caused; the magnitude of this effect depends on the chemical nature of the substituted element. The substitution of one Si by one Al produces a shift in the lines to more positive values between 3 and 5 ppm. This feature is well represented in the chemical shifts of the Q4 units (mAl) in aluminosilicates [19]. Even smaller but still measurable changes (typically ~2 ppm) in the chemical shifts of ^{29}Si result from the presence of crystallographic distortions in the Si polyhedra.

Previous works have studied the geopolymerization reaction using MAS-NMR analysis. Duxson et al. [9] studied the influence of nominal $\text{Na}_2\text{O}/(\text{Na}_2\text{O} + \text{K}_2\text{O})$, and Si/Al ratios on short-range network ordering were assessed using deconvolution analysis of the ^{29}Si MAS-NMR spectra for Na, NaK, and K geopolymers. They found that higher Si/Al ratios caused a shift in the Q4(mAl) positions to more negative chemical shifts. Particularly, K-geopolymers exhibited varying concentrations of Q4(4Al) and Q4(3Al) centers at low Si/Al ratios, indicating distinct ordering patterns depending on the type of alkali present. The relatively lower Q4(4Al) fraction and higher Q4(3Al) fraction in K-geopolymers suggested a comparatively more disordered structure, characterized by the presence of Al-O-Al linkages within the material. Meanwhile, Singh et al. [20] reported the formation of transient aluminum species during the reaction of metakaolin with NaOH, as observed through ^{27}Al MAS-NMR data. Additionally, the interaction between silicate anions and aluminum sites in metakaolin was evident during the synthesis of geopolymers, as indicated by the low-field shift in ^{29}Si MAS-NMR resonance lines of silicate centers. As the reaction progresses, the coordination of aluminum (IV, V, and VI) in metakaolin undergoes a nearly complete transformation to aluminum (IV). Additionally, when selected compositions in the ternary system of sodium silicate, metakaolin, and aqueous alkali are analyzed by ^{29}Si MAS-NMR, geopolymerization is observed in a distinct compositional region. Buchwald [21] et al. conducted a comprehensive investigation into the variability of aluminosilicate gels formed from solutions with distinct batch compositions. Their findings underscore the pivotal influence of two key factors: the Si/Al ratio in the solution and the concentration of NaOH. These factors emerged as critical determinants in aluminosilicate gel formation, shedding light on the intricate nature of the gel-forming process.

Geopolymer foam exhibits a different microstructure characterized by a network of interconnected voids or pores when we compare them to solid geopolymer [22]. This porous structure contributes to its lightweight nature and can influence properties such as permeability [23] and moisture absorption [24,25]. The structure of geopolymer foams has been studied in previous works as well as the influence of foaming agent on the geopolymerization mechanism. Hajimohammadi et al. [26] delved into the influence of aluminum reactions on the phase evolution of fly ash-based geopolymers. Their findings revealed that during the initial stages of geopolymerization, aluminum reactions prompted the formation of aluminum hydroxide gel, which precipitated on fly ash surfaces, masking their reactivity. Consequently, the dissolution rate of fly ash decreased, leading to delayed strength development. However, the increased release of alumina into the solution due to aluminum reactions resulted in better connectivity among unreacted particles and improved microstructural development. By adjusting the ratio of alkali activators, a higher degree of aluminum reaction facilitated faster geopolymer setting, leading to increased

porosity and altered pore size distribution in geopolymer foams, never with any need for additional aluminum powder [27]. Our previous work [28] also explored the influence of foaming agent type and rate, as well as stabilizers, on the thermomechanical behavior of geopolymer foam, further improving our understanding of these materials.

The main focus in this work is on monitoring the geopolymerization reaction of geopolymer foam, using ^{29}Si and ^{27}Al MAS-NMR analysis. Our study involved three different samples, each one aerated with a specific foaming agent: aluminum powder, zinc powder, and hydrogen peroxide. By employing different foaming agents for each sample, we aimed to explore how the variations in the aeration process influenced the geopolymerization reaction and, consequently, the properties of resulting foam materials. Our findings shed light on the intricate geopolymerization kinetics and provide a deeper understanding of the foam's structure–property relationship.

2. Materials and Methods

The materials used in this study include a low calcium content FA classified as Class F according to ASTM C618 [29]. X-ray fluorescence spectroscopy (XRF) was used to analyze the composition of the FA, revealing that it is primarily composed of SiO_2 (53%), Al_2O_3 (30%), and Fe_2O_3 (2.9%). The loss of ignition (LOI) of the FA was found to be 7.1%, as presented in Table 1. The ^{29}Si and ^{27}Al NMR spectra of the initial fly ash, along with their deconvolution, are thoroughly presented in Figure 1 and discussed in our preceding paper [30].

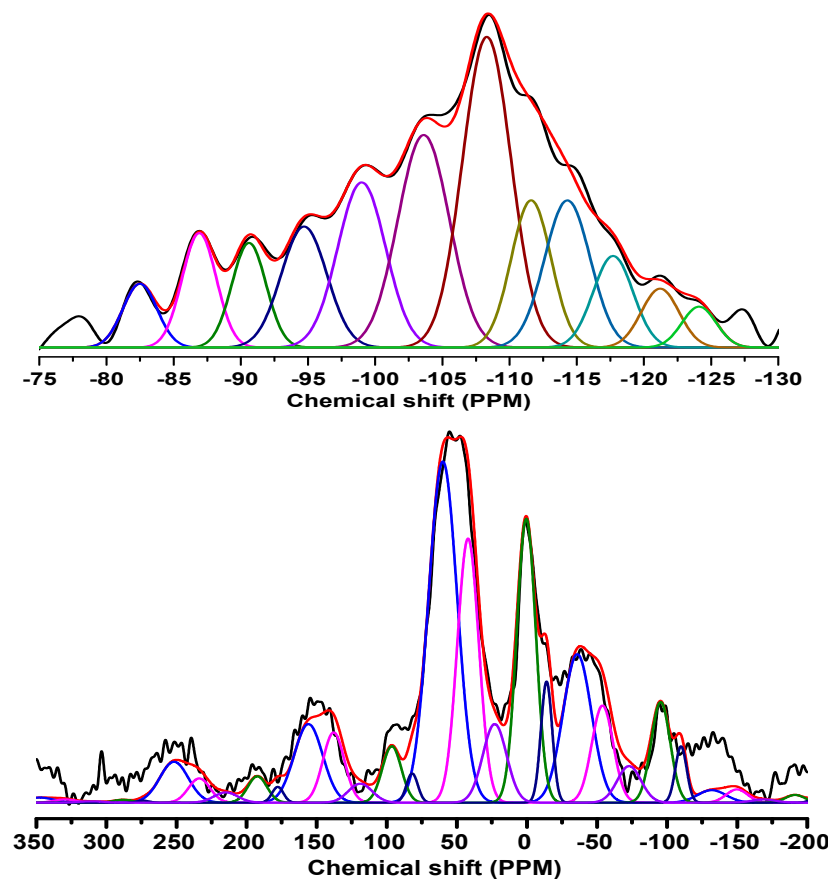


Figure 1. ^{29}Si and ^{27}Al NMR fly ash spectra and their deconvolutions [30].

In addition, a sodium silicate solution (Na_2SiO_3) containing 18% Na_2O and 63% SiO_2 was used. We also employed a 12M solution of sodium hydroxide, which was prepared by dissolving NaOH pellets (purity 97%–99%) in distilled water.

In this study, three common foaming agents were used: aluminum powder [26,27,31,32], zinc powder [28,33,34], and hydrogen peroxide [28,32,35–37]. Aluminum powder is favored for its ability to release hydrogen gas upon reacting with alkaline solutions, contributing to lightweight foam with interconnected voids. Zinc powder, though less used, similarly releases hydrogen gas to aid in foaming. Hydrogen peroxide decomposes releasing oxygen gas, offering control over foam density and pore size. We applied three foaming agents alongside the anionic surfactant sodium dodecyl sulfate (SDS) as the stabilizer, sourced from Sigma-Aldrich with a purity exceeding 90%.

Table 1. Chemical composition of FA.

Oxides	SiO ₂	Al ₂ O ₃	Fe ₂ O ₃	CaO	K ₂ O	Na ₂ O	TiO ₂	SO ₃	MgO	Others
%	52.5	30.2	2.94	0.82	2.08	0.72	1.03	0.79	1.23	0.45
LOI = 7.12										

The formulation selection was based on extensive research conducted in our previous studies. In these studies, we focused on optimizing various parameters, including the initial ratios of fly ash (FA) to alkaline solution, and the ratio of sodium silicate to sodium hydroxide [33], as well as the type of alkaline solution and curing conditions [34,35]. Through systematic experimentation and analysis, we identified the optimum formula that yielded the desired properties for geopolymer foam production, encompassing mechanical, microstructural, and thermal aspects [36]. This optimized formula, which was validated in our previous research, serves as the basis of our current study on geopolymer foam elaboration.

To produce the geopolymer foam samples, we first mixed fly ash, which was classified as Class F, with an alkaline solution. Next, we added a foaming agent, along with the surfactant SDS as a stabilizer, to the resulting paste.

Once the mixtures were thoroughly combined, we poured them into molds and placed them in a ventilated oven at 70 °C for 24 h. After the initial heating, the samples were then left to dry at ambient temperature. Compositions of the samples were presented in Table 2.

Table 2. Compositions of the samples.

	FA	NaOH	Na ₂ SiO ₄	Water	Foaming Agent	Stabilizing
GF-Al1	61.05%	6.98%	17.44%	14.53%	Al powder (0.1%)	0.1%
GF-Z1	61.05%	6.98%	17.44%	14.53%	Zinc Powder (0.1%)	0.1%
GF-H1	61.05%	6.98%	17.44%	14.53%	Hydrogen peroxide (1%)	0.1%

3. Results and Discussion

3.1. Monitoring of Geopolymer foam Geopolymerization Using ²⁷Al MAS NMR

The GF-Al1 sample was monitored by ²⁷Al MAS-NMR at an early age (Figure 2) to follow up the kinetics of the geopolymer foam paste. The GF-Al1 sample was monitored first over the setting time and afterwards day by day until 28 days. The ²⁷Al MAS-NMR spectra for the GF-Al1 sample showed the development of the geopolymer structure at the early stage. During the setting time, NMR signals indicate the presence of both aluminum species in the amorphous and crystalline regions of the sample. As the sample ages, NMR signals become more and more intense and well-defined, suggesting that a more ordered structure is being formed. This indicates that geopolymerization reaction kinetics is proceeding as expected, and that the sample is undergoing a transformation to a solid state.

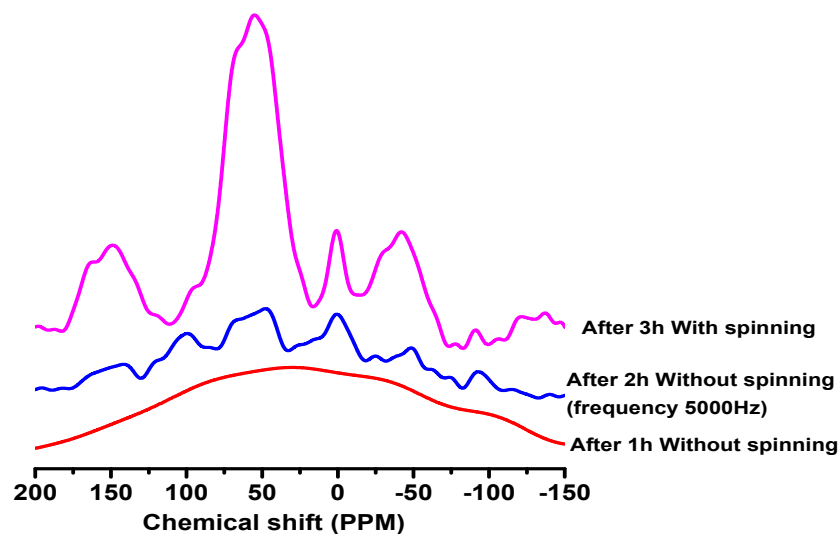


Figure 2. ^{27}Al NMR spectra of GF-A11 at early stage.

After the elaboration, our pastes present a great amount of liquid that make it difficult to conduct MAS-NMR analysis. It is important to note that in liquids, it is not necessary to spin the samples and that NMR spectra obtained in this way with no spinning action present very well resolved components.

The samples were analyzed without spinning after 10 min, but no NMR signal was obtained. This could be due to a number of factors, such as the sample being too inhomogeneous or the sample being too small to generate a measurable NMR signal. However, after 1 h of preparation, a broad signal was obtained, where we could not clearly identify the different environments present at the time; the paste contained many contributions of aluminum species formation, which we could not identify without spinning the sample.

After 2 h, the analysis was performed with spinning at a frequency of 5000 Hz, resulting in peaks with low intensity. This low intensity of the peaks after spinning could have been due to several factors, including poor spinning stability, limited spectral resolution, or low signal-to-noise ratio.

After 3 h, the sample started to harden, and the NMR analysis was performed with spinning at a frequency of 10 kHz. The resulting NMR spectrum showed two main peaks attributed to tetrahedral aluminum (50 ppm) and octahedral aluminum (−1 ppm), as well as spinning sidebands. The presence of two main peaks in the NMR spectrum, one assigned to tetrahedral aluminum and the other to octahedral aluminum, suggests that the sample contains both aluminum species in distinct coordination environments. The spinning sidebands are also a common feature in Al MAS-NMR spectra and result from the interaction between the spinning and the magnetic field gradients in the sample.

The GF-Zn1 sample (Figure 3) became hard faster than Al one and again, an NMR analysis was performed at different times and with different conditions. At 1 h, the sample has a fluid appearance but with inhomogeneities due to the nucleation of different species. Since it was analyzed without spinning, the resulting NMR spectrum was just a broad peak with low intensity and poor spectral resolution. After 2 h, the sample was analyzed with spinning at a frequency of 10 kHz, and the resulting NMR spectrum contained two peaks attributed to tetrahedral aluminum (50 ppm) and octahedral aluminum (−1 ppm), as well as spinning sidebands. NMR analysis with spinning could then provide more detailed information about the Al coordination of the sample. The same behavior was observed for the GF-Zn1 sample (Figure 3) at an early age, with this analysis having been performed after one hour and two hours.

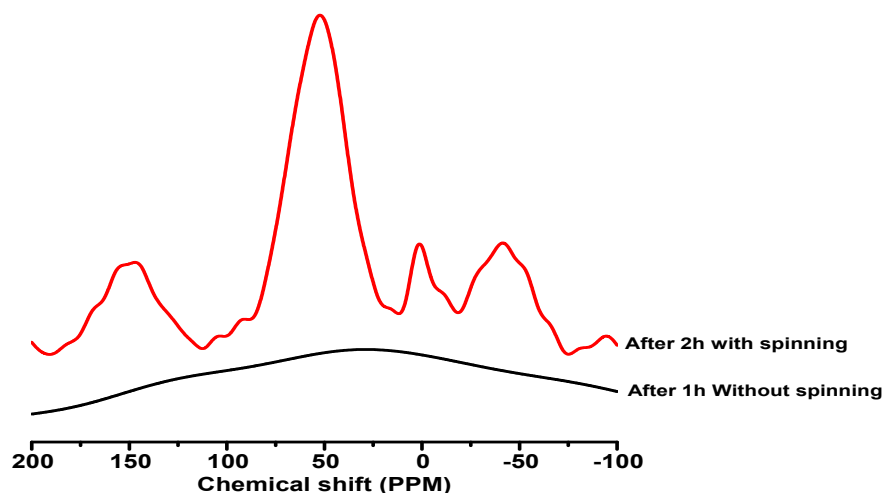


Figure 3. ^{27}Al NMR spectra of GF-Z1 at early stage.

The ^{27}Al MAS-NMR spectra of GF-A11, GF-H1, and GF-Zn1 at 1 day, 3 days, 6 days, 10 days, 15 days, and 28 days are displayed in Figures 4–6. In order to do a semiquantitative study of our samples to investigate the percentage of tetrahedral coordinated aluminum (AlT) and octahedral aluminum (AlO), deconvolution of the ^{27}Al MAS-NMR spectra was carried out using dmfit v68, taking into account the closest spinning side band. Results are reported in Figure 7 and data are presented in Table 3.

The ^{27}Al MAS-NMR spectra of the geopolymer foam samples changed with time as the geopolymerization reaction progressed. It is relevant to note that peaks on the ^{27}Al MAS-NMR spectra were poorly defined and the resolution did not change significantly at 1, 3, and 6 days, because the sample was not well hardened and the geopolymerization reaction was still ongoing [12]. However, after 10, 15, and 28 days, NMR patterns of the three geopolymer foam samples now contained more defined components. The first component was centered at +57 ppm and was related to tetrahedral aluminum [37], while the second one was smaller and centered at +1 ppm, so it was attributed to octahedral aluminum. This suggests that the structure and distribution of aluminum species in the samples changes as the geopolymerization reaction progresses.

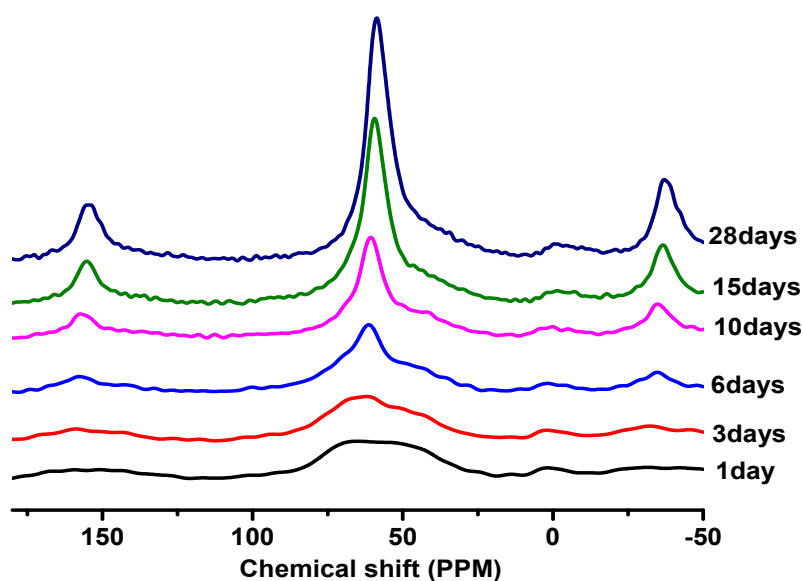


Figure 4. ^{27}Al NMR spectra of GF-A11 after 1, 3, 5, 10, 15, and 28 days.

The main reaction product of the alkaline activation of fly ash is an Al-rich phase (Gel1) [15], consisting of an amorphous gel with a cross-linked aluminosilicate polymer network. Deconvolution of the spectra gives rise to two tetrahedral components (61 and 46 ppm, approximately) and one octahedral component at -3 ppm [37]. The area of the component at 46 ppm decreases with reaction time, while that at 61 ppm increases. This suggests that the Al-rich phase (Gel1) gradually turns into a second Si-rich phase (Gel2) as the reaction continues [38]; there was also an increase in the tetrahedral Al component at 61 ppm.

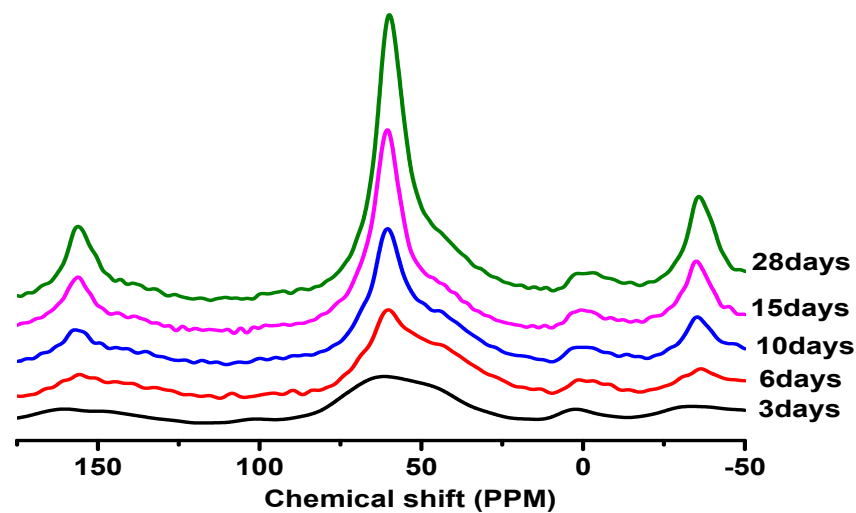


Figure 5. ^{27}Al NMR spectra of GF-H1 after 3, 5, 10, 15, and 28 days.

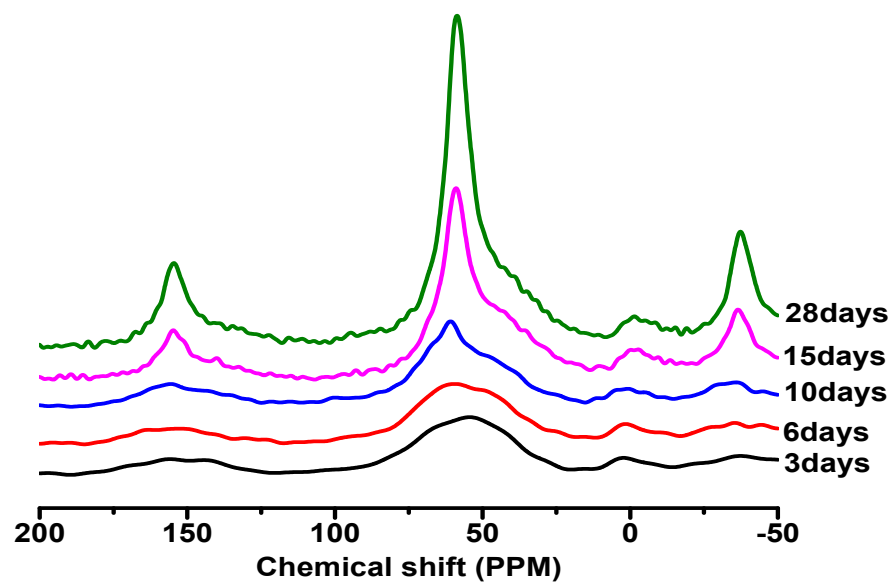


Figure 6. ^{27}Al NMR spectra of GF-Z1 after 3, 5, 10, 15, and 28 days.

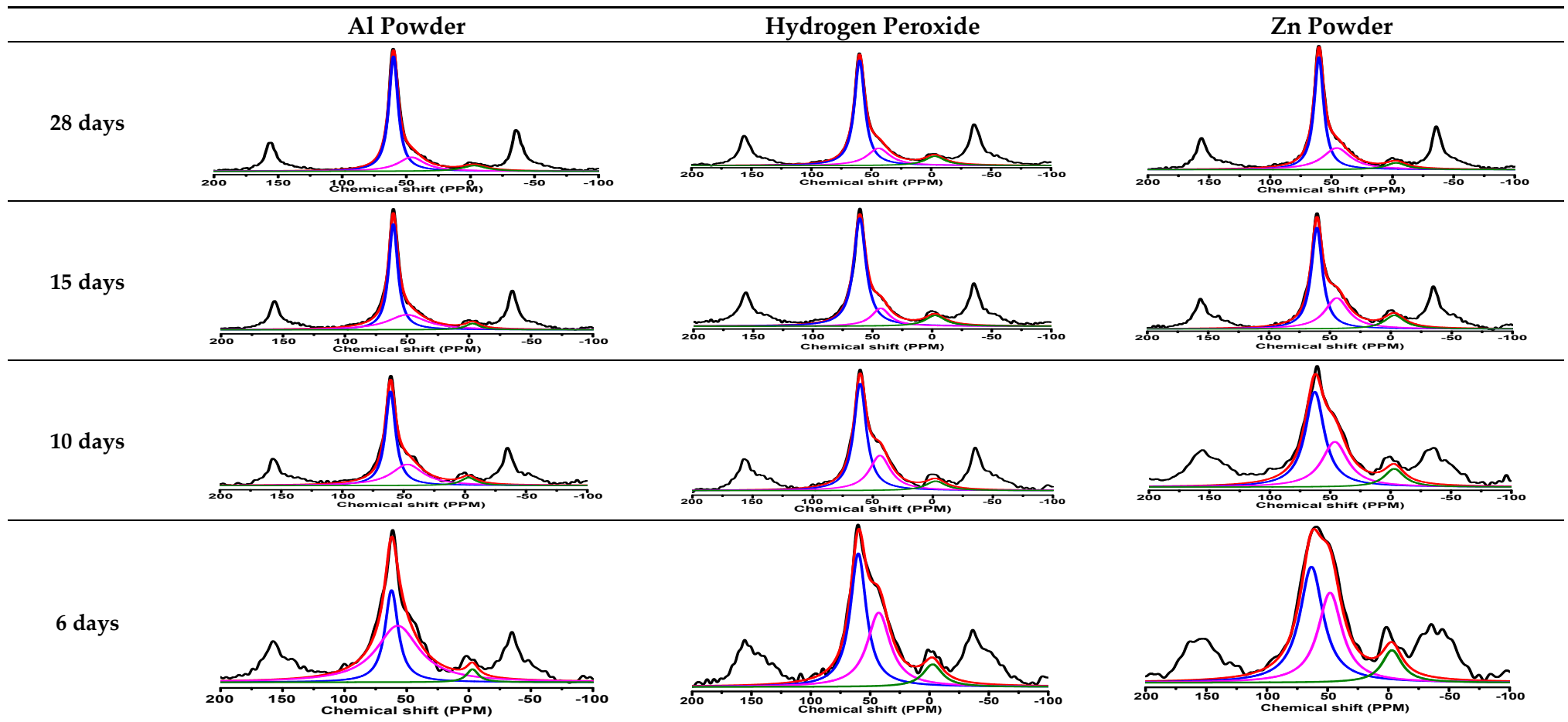


Figure 7. ^{27}Al NMR spectra with deconvolution of GF-Al1, GF-H1, and GF-Zn1 after 6, 10, 15, and 28 days of curing.

Table 3. ^{27}Al MAS-NMR data for the geopolymer foams.

		AIT		AIO
GF-AI1-6 days	d (ppm)	62.20	57.25	−3
	%	38.55	58.51	2.93
GF-AI1-10 days	d (ppm)	60.93	47.0	−3.0
	%	61.68	33.62	4.70
GF-AI1-15 days	d (ppm)	61.02	50.00	−3.0
	%	66.40	30.03	3.57
GF-AI1-28 days	d (ppm)	60.04	46.01	−3.0
	%	74.05	20.41	5.55
GF-H1-6 days	d (ppm)	60.00	42.75	−2.64
	%	56.58	36.43	6.99
GF-H1-10 days	d (ppm)	60.51	43.94	−2.45
	%	65.18	29.40	5.42
GF-H1-15 days	d (ppm)	60.62	43.00	−2.61
	%	77.08	15.50	7.42
GF-H1-28 days	d (ppm)	59.73	43.80	−3.00
	%	72.19	20.59	7.22
GF-Z1-6days	d (ppm)	63.32	48.00	−3.00
	%	55.77	36.27	7.96
GF-Z1-10 days	d (ppm)	62.81	46.19	−3.00
	%	56.74	36.39	6.87
GF-Z1-15 days	d (ppm)	60.74	44.37	−3.00
	%	60.37	31.02	8.61
GF-Z1-28 days	d (ppm)	60.16	45.58	−3.00
	%	65.93	29.09	4.97

3.2. Monitoring of the Geopolymerization Process of Geopolymer Foam Using ^{29}Si MAS-NMR

The ^{29}Si MAS-NMR spectra of GF-AI1, GF-H1, and GF-Zn1 geopolymer foam samples are presented in Figures 8 and 9, and results are summarized in Table 4. The spectra of the three samples show broad and poorly resolved bands at the early stages of the reaction, due to short reaction times and unreacted FA, indicating a high degree of disorder. The broad peak observed was in the chemical shift range of -70 to -120 ppm, which is a characteristic feature of both aluminosilicates and silica gels [39]. However, as the reaction time increases, the intense peaks shift towards higher chemical shifts, indicating the ongoing geopolymerization reaction of the geopolymeric foams [40]. The principal reaction product in all analyzed geopolymer foam samples is an alkali aluminosilicate gel [41]. The spectra have been deconvoluted to identify the various Qn species, which provide information about the degree of polymerization and the ordering of the geopolymer foam [12].

The ^{29}Si MAS-NMR spectra for the geopolymer foam cured at different reaction times exhibited three overlapping areas. The spectra contained a large profile including several peaks shown after deconvolution. The one on the left could be fitted to the components in the -66 ppm to -72 ppm range, given the presence of Q0 monomers attributable to depolymerization products. The peaks detected in the middle zone at ~ -80.00 ppm and -86 ppm were attributed to the Q1 and Q2 units, indicating the presence of a N-A-S-H-like gel [42]. The band at around -91 ppm was associated with Q3(1Al) units. In the third zone,

peaks at approximately -95 , -99 , -104 , and -109 ppm were associated with Q3/Q4(3Al), Q4(2Al), Q4(1Al), and Q4(0Al), respectively [15,40,43]; Q4(4Al) overlaps with the Q3(1Al) signal. The presence of these components is indicative of a N-(C)-A-S-H-like gels [44], characterized by a highly polymerized aluminosilicate structure in which Si and Al were tetrahedrally coordinated. Signal width decreases as reaction time increases; this effect may be associated with a higher ordering of the gels formed. In addition, the peaks detected around -115 and -122 ppm were attributed to the silica crystalline phase of the starting material and to the unreacted glassy phase Si-O-Si of the unreacted FA [45–47]. Considering the overlap between FA and N-A-S-H gel signals and the high noise level, components in this right-hand area of the spectrum are difficult to assign with any accuracy. The size of this area declined over time (from 10 to 28 days), probably attributed to FA, although possible N-A-S-H formation cannot be ruled out. The middle zone associated with C-A-S-H and (N, C)-A-S-H gels, in contrast, was observed to grow with reaction time.

The ^{29}Si NMR spectrum can provide information about the condensation reactions in geopolymer foam synthesis, and the peak shifts observed can be used to estimate the extent of Si-O-Al link formation [9].

After 15 days of reaction, the peak assigned to Q2 at -86 ppm was more intense in GF-Al1 and GF-H1 compared to GF-Z1, suggesting a higher degree of polymerization and ordering in GF-Al1 [26] and GF-H1 samples. The continuous change over 28 days found suggests that the time for the completion of silicate condensation may be very long.

Condensation reactions usually involve both aluminate and silicate species, as well as silicate species alone [48]. However, since alkaline sodium silicates are used as activators, the apparent Si content in the gel phase is usually higher than the Al content. Consequently, most of the condensation reactions in the geopolymer foam synthesis process involve silicate species. The higher degree of condensation of geopolymer foam corresponds to a higher proportion of Q2 and Q3 species and a lower proportion of Q0 and Q1 species [37]. The sample GF-Al1 has the highest degree of condensation with 24% Q2 species and 9% Q3 species, while GF-H1 has a slightly lower degree of condensation with 19.6% Q2 species and 12% Q3 species. The sample GF-Z1 has the lowest degree of condensation with 17% Q2 species and 8% Q3 species. The higher degree of condensation observed in the sample GF-Al1 is due to the higher content of Al species in the gel phase, which has a positive effect on the rate of condensation [48].

GF-Z1 also required a longer time for gel production compared to GF-Al and GF-H1. Analysis of the ^{29}Si MAS-NMR spectra revealed that the most thermodynamically stable final compound was achieved after 15 days with a minimal difference after 28 days in the geopolymer foam pastes. The amount of ash remaining at the end of the geopolymerization reaction is related to the degree of condensation [49,50], which is a measure of the extent to which the starting materials have reacted to form the geopolymer network. A higher degree of condensation means that more of the available chemical bonds have been used to form the geopolymer network, resulting in a more complete reaction and fewer unreacted materials remaining as ash.

In the case of the sample GF-Z1, the higher amount of ash remaining at the end of the reaction is likely due to a lower degree of condensation compared to the other samples. This could be because using of zinc powder as a foaming agent, as mentioned earlier, can impact the condensation degree of the geopolymerization reaction. On the other hand, samples GH-Al1 and GF-H1 may have had a higher degree of condensation, and therefore a lower amount of ash remaining at the end of the reaction. The exact reasons for the differences in degree of condensation and ash content between the samples would depend on the specific experimental conditions and starting materials used.

Using aluminum powder and hydrogen peroxide as foaming agents can indeed impact the geopolymerization reaction [26]. Aluminum powder can react with the alkali solution used in the geopolymerization process, thus producing hydrogen gas, which results in the formation of pores and increases the porosity of the final product [31,51,52]. Hydrogen peroxide can also release oxygen gas during the reaction, which can further contribute to

the foaming process [53]. The use of these foaming agents can have a positive effect on the geopolymerization reaction by promoting foaming and increasing the porosity of the final product. In addition, the foaming process can also lead to a higher degree of condensation in the geopolymerization reaction. This is because the foaming can help to create a more open and interconnected pore structure [54], which can facilitate the formation of the geopolymer network. However, the use of aluminum powder and hydrogen peroxide as foaming agents in geopolymerization reactions can have positive effects on the final product by promoting foaming, increasing porosity, and leading to a higher degree of condensation. In addition, the low amount of ash remaining at the end of the reaction can further enhance the quality of the final product.

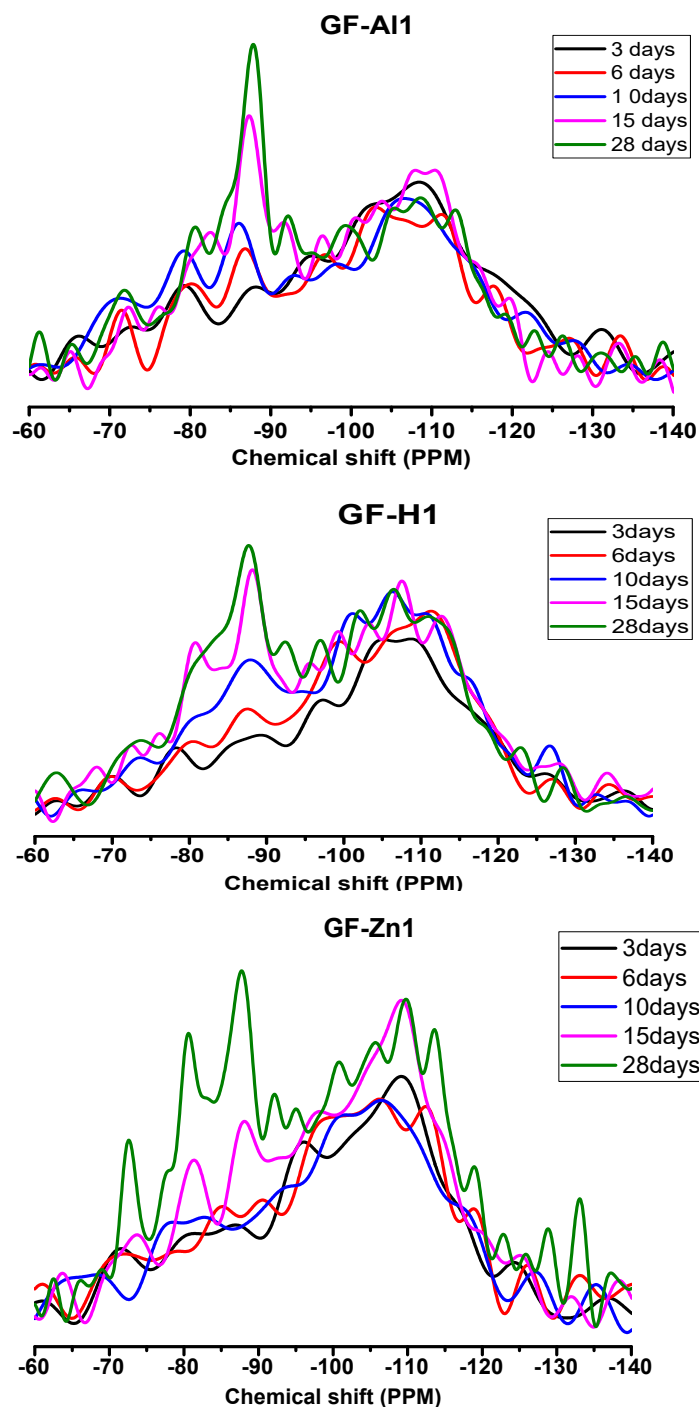


Figure 8. ²⁹Si NMR spectra of GF-AI1, GF-H1, and GF-Zn1.

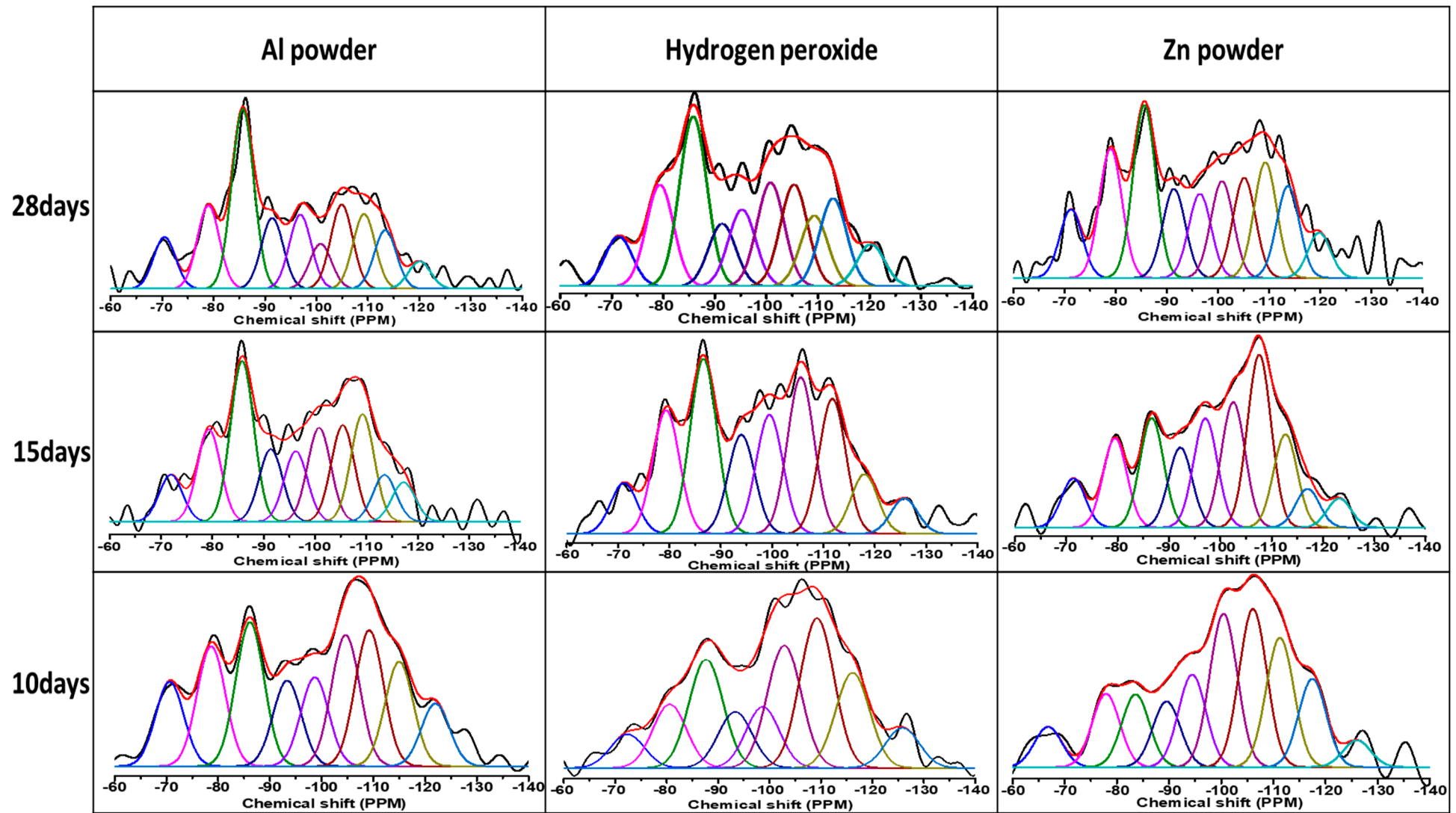


Figure 9. ^{29}Si NMR spectra with deconvolution of GF-Al1, GF-H1, and GF-Zn1 after 10, 15, and 28 days of curing.

Table 4. ^{29}Si MAS NMR data for the geopolymer foam samples.

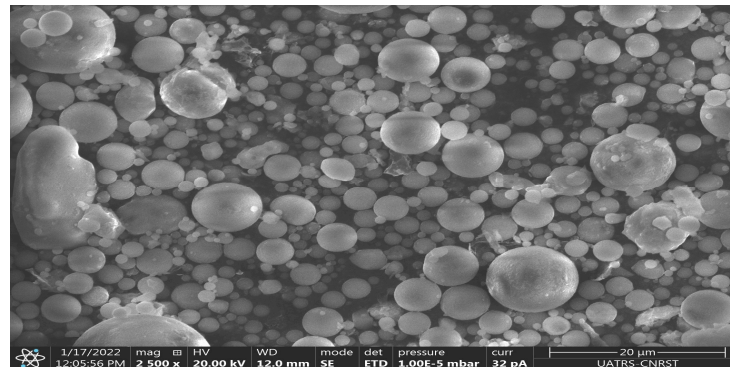
		Q0	Q1	Q2	Q3(1Al) and Q4(4Al)	Q3 and Q4(3Al)	Q4(2Al)	Q4(1Al)	Q4(0Al)	Remnant SiO ₂	Remnant FA
GF-A11-10 days	δ (ppm)	−70.63	−78.65	−86.14		−93.34	−98.67	−104.63	−109.24	−114.99	−122.98
	%	8.77	12.56	15.13		8.91	9.17	13.79	14.27	10.88	6.52
GF-A11-15 days	δ (ppm)	−71.96	−79.36	−85.81	−91.40	−96.25	−100.80	−105.40	−109.25	−113.52	−117.25
	%	5.67	11.16	19.46	8.78	8.52	11.36	11.66	12.99	5.65	4.75
GF-A11-28 days	δ (ppm)	−70.46	−78.99	−85.68	−91.40	−96.86	−100.80	−104.90	−109.25	−113.38	−120.04
	%	6.87	11.14	23.98	9.44	9.86	5.99	11.22	9.98	7.84	3.66
GF-H1-10 days	δ (ppm)	−72.37	−80.58	−87.67		−93.34	−98.67	−102.87	−109.24	−116.17	−125.86
	%	4.61	8.68	14.85		7.66	8.26	16.84	20.60	13.02	5.48
GF-H1-15 days	δ (ppm)	−71.16	−79.37	−86.64		−94.02	−99.49	−105.59	−111.75	−118.0	−125.77
	%	5.32	12.95	18.34		10.39	12.48	16.43	14.16	6.25	3.69
GF-H1-28 days	δ (ppm)	−71.34	−79.34	−85.79	−91.40	−95.26	−100.80	−105.33	−109.25	−112.91	−120.24
	%	5.75	11.71	19.62	7.22	11.98	11.98	11.74	8.14	10.13	4.85
GF-Z1-10 days	δ (ppm)	−66.83	−77.91	−83.58	−89.52	−94.43	−100.43	−106.08	−111.25	−117.47	−126.72
	%	4.44	8.09	8.05	7.26	10.22	17.11	17.65	14.44	9.77	2.97
GF-Z1-15 days	δ (ppm)	−71.38	−79.49	−86.64	−92.21	−97.10	−102.51	−107.58	−112.68	−117.91	−123.15
	%	5.47	9.96	12.23	8.92	12.19	14.00	19.31	10.39	4.31	3.23
GF-Z1-28 days	δ (ppm)	−71.29	−79.04	−85.61	−91.40	−96.46	−100.80	−105.12	−109.25	−113.67	−119.79
	%	6.90	13.01	17.39	8.96	8.45	9.76	10.06	11.64	9.27	4.56

The use of zinc powder as a foaming agent can indeed impact the geopolymerization reaction. Zinc powder can act as a reducing agent, which can reduce the oxidation state of some of the cations present in the starting materials used to make the geopolymer. This reduction can affect the condensation degree of the geopolymerization reaction [55], meaning that fewer of the available chemical bonds will be used to form the geopolymer network. As a result, the resulting geopolymer may have a lower degree of polymerization, which can lead to weaker mechanical properties. In addition to affecting the condensation degree, the use of zinc powder can also result in a high amount of ash remaining at the end of the reaction. This is because the reduction of cations can lead to the formation of excess unreacted materials that do not contribute to the geopolymer network. These unreacted materials can be found in the final product as ash, which can affect the properties of the geopolymer. Overall, the use of zinc powder as a foaming agent in geopolymerization reactions can have both positive and negative effects. While it can promote foaming and improve the porosity of the resulting material, it can also impact the condensation degree and result in a high amount of ash remaining at the end of the reaction. These effects should be carefully considered when using zinc powder as a foaming agent in geopolymerization reactions.

3.3. Scanning Electron Microscopy

In Figure 10, SEM images of FA and geopolymer foam samples GF-A11-28 days, GF-H1-28days, and GF-Z1-28 days are presented. We noted the presence of unreacted fly ash particles, which were more pronounced in the samples aerated with Al powder and zinc powder compared to those aerated with H_2O_2 . This discrepancy can be attributed to the rapid reaction kinetics between Al powder and the alkaline activator, leading to a faster consumption of reactive components and a higher content of unreacted fly ash particles. In contrast, H_2O_2 , as a foaming agent, may not induce such rapid reactions, resulting in a more complete consumption of fly ash particles during the geopolymerization process.

FA



GF-A11-28days



Figure 10. Cont.

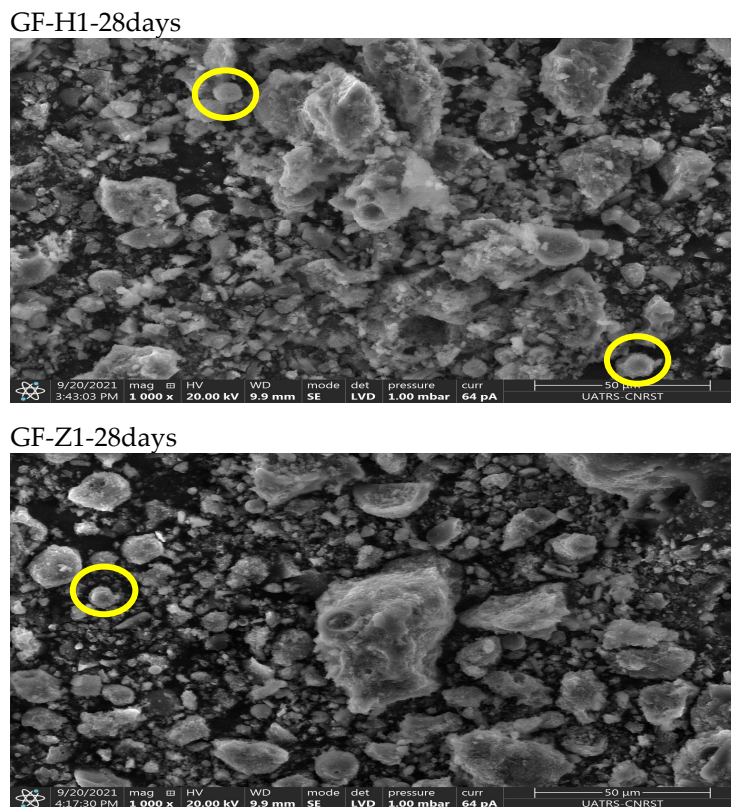


Figure 10. SEM images of FA, GF-A11-28 days, GFHZ1-28 days, and GF-Z1-28 days.

3.4. Foaming Mechanism

The foaming mechanism in geopolymerization involves generating and stabilizing bubbles within the geopolymer matrix. This process typically incorporates foaming agents into the geopolymer mixture. Here is an overview of the foaming mechanism in the geopolymerization process system: When the foaming agent is introduced into the geopolymer mixture, it undergoes a reaction or decomposition that releases gas. For instance, hydrogen peroxide decomposes into water (H_2O) and oxygen gas (O_2), while aluminum powder/zinc powder reacts with alkaline solutions to produce hydrogen gas (H_2). These gases create bubbles within the mixture. Stabilizing these bubbles is crucial to prevent coalescence and collapse. We utilized SDS surfactant in our samples, which adsorbs onto bubble surfaces, reducing surface tension and stabilizing them. The foamed geopolymer mixture is then cast or molded into the desired shape and allowed to cure. During curing, the geopolymer precursor materials undergo polycondensation reactions, forming a three-dimensional network of bonded molecules. The stabilized bubbles become trapped within this network, creating a cellular structure in the final geopolymer material. In our study, we noted that the foaming agent influenced the geopolymerization process; we observed that the gel produced in samples aerated using zinc powder exhibited a slower geopolymerization reaction compared to other foaming agents utilized. This observation suggests that the choice of foaming agent can significantly impact both the rate and stability of the geopolymerization steps, thereby influencing the properties of the final geopolymer material.

4. Conclusions

This study aimed to investigate the impact of various foaming agents on the geopolymerization reaction in order to produce geopolymer foam. To accomplish this, ^{27}Al and ^{29}Si magic angle spinning NMR techniques were employed to monitor the reaction's development over time. However, detecting changes at the early stage of the reaction was

challenging, since the ^{27}Al MAS-NMR analysis requires 30 min, and the ^{29}Si MAS-NMR requires more than 2 h to complete the acquisition of the spectra.

This study discovered that using zinc powder as the foaming agent slowed down the geopolymerization reaction of the geopolymer foam. The ^{29}Si MAS-NMR results indicate that peaks attributed to the gel's production appeared later than in samples produced using aluminum powder and hydrogen peroxide. Overall, these findings provide valuable insights for using different foaming agents in geopolymerization reactions to produce geopolymer foam. Further research could focus on optimizing the reaction conditions and exploring other potential foaming agents to improve the foam quality and properties.

Author Contributions: Conceptualization, G.M. and I.S.; formal analysis, G.M. and I.S.; investigation, G.M., I.S., S.A. and M.T.; writing—original draft preparation, G.M. and I.S.; writing—review and editing, G.M., I.S., S.A. and M.T.; All authors have read and agreed to the published version of the manuscript.

Funding: This research received no external funding.

Data Availability Statement: The authors confirm that the data generated or analyzed during this study are provided in full within the published article.

Acknowledgments: The authors acknowledge the support of Virginia Diez-Gómez from ICMM/CSIC for helping in performing MAS-NMR analysis.

Conflicts of Interest: The authors declare no conflicts of interest.

References

1. Davidovits, J. Geopolymers: Inorganic Polymeric New Materials. *J. Therm. Anal.* **1991**, *37*, 1633–1656. [[CrossRef](#)]
2. Castillo, H.; Collado, H.; Droguett, T.; Vesely, M.; Garrido, P.; Palma, S. State of the Art of Geopolymers: A Review. *E-Polym.* **2022**, *22*, 108–124. [[CrossRef](#)]
3. Kobera, L.; Brus, J.; Klein, P.; Dedecek, J.; Urbanova, M. Biaxial Q-Shearing of ^{27}Al 3QMAS NMR Spectra: Insight into the Structural Disorder of Framework Aluminosilicates. *Solid State Nucl. Magn. Reson.* **2014**, *57–58*, 29–38. [[CrossRef](#)] [[PubMed](#)]
4. Brus, J.; Abbrent, S.; Kobera, L.; Urbanova, M.; Cuba, P. Advances in ^{27}Al MAS NMR Studies of Geopolymers. In *Annual Reports on NMR Spectroscopy*; Elsevier: Amsterdam, The Netherlands, 2016; Volume 88, pp. 79–147. ISBN 978-0-12-804713-2.
5. Gupta, R.; Tomar, A.S.; Mishra, D.; Sanghi, S.K. Multinuclear MAS NMR Characterization of Fly-Ash-Based Advanced Sodium Aluminosilicate Geopolymer: Exploring Solid-State Reactions. *ChemistrySelect* **2020**, *5*, 4920–4927. [[CrossRef](#)]
6. Engelhardt, G.; Michel, D. *High-Resolution Solid-State NMR of Silicates and Zeolites*; Wiley: Hoboken, NJ, USA, 1987.
7. Schneider, J.; Mastelaro, V.R.; Panepucci, H.; Zanotto, E.D. ^{29}Si MAS-NMR Studies of Qn Structural Units in Metasilicate Glasses and Their Nucleating Ability. *J. Non Cryst. Solids* **2000**, *273*, 8–18. [[CrossRef](#)]
8. Stebbins, J.F.; Xue, X. NMR Spectroscopy of Inorganic Earth Materials. *Rev. Mineral. Geochem.* **2014**, *78*, 605–653. [[CrossRef](#)]
9. Duxson, P.; Provis, J.L.; Lukey, G.C.; Separovic, F.; van Deventer, J.S.J. ^{29}Si NMR Study of Structural Ordering in Aluminosilicate Geopolymer Gels. *Langmuir* **2005**, *21*, 3028–3036. [[CrossRef](#)]
10. Chen, X.; Sutrisno, A.; Struble, L.J. Effects of Calcium on Setting Mechanism of Metakaolin-Based Geopolymer. *J. Am. Ceram. Soc.* **2018**, *101*, 957–968. [[CrossRef](#)]
11. Yasmin, T.; Müller, K. Synthesis and Surface Modification of Mesoporous Mcm-41 Silica Materials. *J. Chromatogr. A* **2010**, *1217*, 3362–3374. [[CrossRef](#)]
12. Greiser, S.; Hunger, M.; Jäger, C. ^{29}Si { ^{27}Al } TRAPDOR MAS NMR to Distinguish Qn(mAl) Sites in Aluminosilicates. Test Case: Faujasite-Type Zeolites. *Solid State Nucl. Magn. Reson.* **2016**, *79*, 6–10. [[CrossRef](#)] [[PubMed](#)]
13. Walkley, B.; Provis, J.L. Solid-State Nuclear Magnetic Resonance Spectroscopy of Cements. *Mater. Today Adv.* **2019**, *1*, 100007. [[CrossRef](#)]
14. Bhardwaj, P.; Gupta, R.; Mishra, D.; Mudgal, M.; Amritphale, S.S. ^{27}Al NMR MAS Spectral Studies Inferring the Initiation of Geopolymerization Reaction on Together Mechanochemical Grinding of Raw Materials. *J. Chin. Chem. Soc.* **2018**, *65*, 485–489. [[CrossRef](#)]
15. Palomo, A.; Alonso, S.; Fernandez-Jiménez, A.; Sobrados, I.; Sanz, J. Alkaline Activation of Fly Ashes: NMR Study of the Reaction Products. *J. Am. Ceram. Soc.* **2004**, *87*, 1141–1145. [[CrossRef](#)]
16. Oestrike, R.; Yang, W.; Kirkpatrick, R.J.; Hervig, R.L.; Navrotsky, A.; Montez, B. High-Resolution ^{23}Na , ^{27}Al and ^{29}Si NMR Spectroscopy of Framework Aluminosilicate Glasses. *Geochim. Cosmochim. Acta* **1987**, *51*, 2199–2209. [[CrossRef](#)]
17. MacKenzie, K.J.D.; Smith, M.E. *Multinuclear Solid-State NMR of Inorganic Materials*; Pergamon: Oxford, UK; New York, NY, USA, 2002; ISBN 978-0-08-043787-3.
18. Lippmaa, E.; Maegi, M.; Samoson, A.; Tarmak, M.; Engelhardt, G. Investigation of the Structure of Zeolites by Solid-State High-Resolution Silicon-29 NMR Spectroscopy. *J. Am. Chem. Soc.* **1981**, *103*, 4992–4996. [[CrossRef](#)]

19. Palomo, A.; Macias, A.; Blanco, M.T.; Puertas, F. Physical, Chemical and Mechanical Characterization of Geopolymers. In Proceedings of the 9th International Congress on the Chemistry of Cement, New Delhi, India, 29 October 1992; Volume 5, pp. 505–511.
20. Singh, P.S.; Bastow, T.; Trigg, M. Structural Studies of Geopolymers by ^{29}Si and ^{27}Al MAS-NMR. *J. Mater. Sci.* **2005**, *40*, 3951–3961. [[CrossRef](#)]
21. Buchwald, A.; Zellmann, H.-D.; Kaps, C. Condensation of Aluminosilicate Gels—Model System for Geopolymer Binders. *J. Non-Cryst. Solids* **2011**, *357*, 1376–1382. [[CrossRef](#)]
22. Zhang, Z.; Provis, J.L.; Reid, A.; Wang, H. Geopolymer Foam Concrete: An Emerging Material for Sustainable Construction. *Constr. Build. Mater.* **2014**, *56*, 113–127. [[CrossRef](#)]
23. Papa, E.; Landi, E.; Miccio, F.; Medri, V. K_2O -Metakaolin-Based Geopolymer Foams: Production, Porosity Characterization and Permeability Test. *Materials* **2022**, *15*, 1008. [[CrossRef](#)] [[PubMed](#)]
24. Weng, A.; Wan, X.; Hu, J.; Zhang, S.; Han, S.; Du, Z.; Chen, D.; Zhao, Y. Study of the Control and Influence of Humidity on the Mechanical and Structural Properties of Geopolymer Foam Composites Based on Fly Ash and Wood Flour. *Mater. Lett.* **2024**, *365*, 136443. [[CrossRef](#)]
25. Chi, H.L.; Hájková, P.; Le Van, S.; Louda, P.; Voleský, L. Water Absorption Properties of Geopolymer Foam after Being Impregnated with Hydrophobic Agents. *Materials* **2019**, *12*, 4162. [[CrossRef](#)] [[PubMed](#)]
26. Hajimohammadi, A.; Ngo, T.; Mendis, P. How Does Aluminium Foaming Agent Impact the Geopolymer Formation Mechanism? *Cem. Concr. Compos.* **2017**, *80*, 277–286. [[CrossRef](#)]
27. Hajimohammadi, A.; Ngo, T.; Mendis, P.; Sanjayan, J. Regulating the Chemical Foaming Reaction to Control the Porosity of Geopolymer Foams. *Mater. Des.* **2017**, *120*, 255–265. [[CrossRef](#)]
28. Moutaoukil, G.; Sobrados, I.; Alehyen, S.; Taibi, M. Understanding the Thermomechanical Behavior of Geopolymer Foams: Influence of Rate and Type of Foaming Agent and Stabilizer. *Chem. Data Collect.* **2024**, *50*, 101111. [[CrossRef](#)]
29. ASTM C618; Specification for Coal Fly Ash and Raw or Calcined Natural Pozzolan for Use in Concrete. ASTM International: West Conshohocken, PA, USA, 2019.
30. Moutaoukil, G.; Alehyen, S.; Sobrados, I.; El Mahdi Safhi, A. Effects of Elevated Temperature and Activation Solution Content on Microstructural and Mechanical Properties of Fly Ash-Based Geopolymer. *KSCE J. Civ. Eng.* **2023**, *27*, 2372–2384. [[CrossRef](#)]
31. Wattanasiriwech, D.; Yomthong, K.; Wattanasiriwech, S. Characterisation and Properties of Class C-Fly Ash Based Geopolymer Foams: Effects of Foaming Agent Content, Aggregates, and Surfactant. *Constr. Build. Mater.* **2021**, *306*, 124847. [[CrossRef](#)]
32. Masi, G.; Rickard, W.D.A.; Vickers, L.; Bignozzi, M.C.; van Riessen, A. A Comparison between Different Foaming Methods for the Synthesis of Light Weight Geopolymers. *Ceram. Int.* **2014**, *40*, 13891–13902. [[CrossRef](#)]
33. Moutaoukil, G.; Alehyen, S.; Sobrados, I.; Fadil, M.; Taibi, M. Optimization of Compressive Strength of Fly Ash-Based Geopolymers Using Central Composite Design. *Bull. Mater. Sci.* **2021**, *44*, 138. [[CrossRef](#)]
34. Moutaoukil, G.; Alehyen, S.; Sobrados, I.; Fadil, M.; Taibi, M. Effects of Temperature, Time and Alkaline Solution Content on the Mechanical Properties of Class C Fly Ash-Based Geopolymer Using Taguchi Method. *Moroc. J. Chem.* **2023**, *11*, 11–76. [[CrossRef](#)]
35. Moutaoukil, G.; Alehyen, S.; Sobrados, I.; Taibi, M. Microstructural and ^{29}Si and ^{27}Al MAS NMR Spectroscopic Evaluations of Alkali Cation and Curing Effects on Class C Fly Ash-Based Geopolymer. *Chem. Data Collect.* **2022**, *41*, 100898. [[CrossRef](#)]
36. Moutaoukil, G.; Sobrados, I.; Alehyen, S. Study of Thermomechanical Properties of Foamed and Unfoamed Fly Ash-Based Geopolymer Using FT Raman Spectroscopy and ^{29}Si MAS NMR. *Mater. Lett.* **2023**, *330*, 133261. [[CrossRef](#)]
37. Glid, M.; Sobrados, I.; Rhaïem, H.B.; Sanz, J.; Amara, A.B.H. Alkaline Activation of Metakaolin-Silica Mixtures: Role of Dissolved Silica Concentration on the Formation of Geopolymers. *Ceram. Int.* **2017**, *43*, 12641–12650. [[CrossRef](#)]
38. Criado Sanz, M. Nuevos Materiales Cementantes Basados en la Activación Alcalina de Cenizas Volantes: Caracterización de geles N-A-S-H en Función del Contenido de Sílice Soluble: Efecto Del Na_2SO_4 . Ph.D. Thesis, Universidad Autonoma de Madrid, Madrid, Spain, 2007.
39. Lutz, W.; Heidemann, D.; Hübert, C.; Wieker, W. Contribution of Silica Gels to Superimposed ^{29}Si MAS NMR Spectra of Y Zeolites Dealuminated by Steaming. *Z. Für Anorg. Allg. Chem.* **2001**, *627*, 2559–2564. [[CrossRef](#)]
40. Park, S.-M.; Jang, J.-G.; Chae, S.-A.; Lee, H.-K. An NMR Spectroscopic Investigation of Aluminosilicate Gel in Alkali-Activated Fly Ash in a CO_2 -Rich Environment. *Materials* **2016**, *9*, 308. [[CrossRef](#)] [[PubMed](#)]
41. Fernández-Jiménez, A.; Palomo, A.; Sobrados, I.; Sanz, J. The Role Played by the Reactive Alumina Content in the Alkaline Activation of Fly Ashes. *Microporous Mesoporous Mater.* **2006**, *91*, 111–119. [[CrossRef](#)]
42. Fang, G.; Zhang, M. Multiscale Micromechanical Analysis of Alkali-Activated Fly Ash-Slag Paste. *Cem. Concr. Res.* **2020**, *135*, 106141. [[CrossRef](#)]
43. Fernandezjimenez, A.; Delatorre, A.; Palomo, A.; Lopezolmo, G.; Alonso, M.; Aranda, M. Quantitative Determination of Phases in the Alkali Activation of Fly Ash. Part I. Potential Ash Reactivity. *Fuel* **2006**, *85*, 625–634. [[CrossRef](#)]
44. Criado, M.; Aperador, W.; Sobrados, I. Microstructural and Mechanical Properties of Alkali Activated Colombian Raw Materials. *Materials* **2016**, *9*, 158. [[CrossRef](#)] [[PubMed](#)]
45. Criado, M.; Fernández-Jiménez, A.; Palomo, A. Alkali Activation of Fly Ash: Effect of the $\text{SiO}_2/\text{Na}_2\text{O}$ Ratio. *Microporous Mesoporous Mater.* **2007**, *106*, 180–191. [[CrossRef](#)]
46. Jeon, D.; Jun, Y.; Jeong, Y.; Oh, J.E. Microstructural and Strength Improvements through the Use of Na_2CO_3 in a Cementless $\text{Ca}(\text{OH})_2$ -Activated Class F Fly Ash System. *Cem. Concr. Res.* **2015**, *67*, 215–225. [[CrossRef](#)]

47. Jang, J.G.; Lee, H.K. Effect of Fly Ash Characteristics on Delayed High-Strength Development of Geopolymers. *Constr. Build. Mater.* **2016**, *102*, 260–269. [[CrossRef](#)]
48. Sagoe-Crentsil, K.; Weng, L. Dissolution Processes, Hydrolysis and Condensation Reactions during Geopolymer Synthesis: Part II. High Si/Al Ratio Systems. *J. Mater. Sci.* **2007**, *42*, 3007–3014. [[CrossRef](#)]
49. Ranjbar, N.; Kuenzel, C.; Spangenberg, J.; Mehrali, M. Hardening Evolution of Geopolymers from Setting to Equilibrium: A Review. *Cem. Concr. Compos.* **2020**, *114*, 103729. [[CrossRef](#)]
50. Ranjbar, N.; Kuenzel, C. Influence of Preheating of Fly Ash Precursors to Produce Geopolymers. *J. Am. Ceram. Soc.* **2017**, *100*, 3165–3174. [[CrossRef](#)]
51. Novais, R.M.; Pullar, R.C.; Labrincha, J.A. Geopolymer Foams: An Overview of Recent Advancements. *Prog. Mater. Sci.* **2019**, *109*, 100621. [[CrossRef](#)]
52. Ariffin, N.; Abdullah, M.M.A.B.; Postawa, P.; Zamree Abd Rahim, S.; Mohd Arif Zainol, M.R.R.; Putra Jaya, R.; Śliwa, A.; Omar, M.F.; Wysocki, J.J.; Bloch, K.; et al. Effect of Aluminium Powder on Kaolin-Based Geopolymer Characteristic and Removal of Cu²⁺. *Materials* **2021**, *14*, 814. [[CrossRef](#)] [[PubMed](#)]
53. Boros, A.; Korim, T. Development of Geopolymer Foams for Multifunctional Applications. *Crystals* **2022**, *12*, 386. [[CrossRef](#)]
54. Stochero, N.P.; de Souza Chami, J.O.R.; Souza, M.T.; de Moraes, E.G.; de Oliveira, A.P.N. Green Glass Foams from Wastes Designed for Thermal Insulation. *Waste Biomass Valorization* **2021**, *12*, 1609–1620. [[CrossRef](#)]
55. Kim, T.; Kang, C.; Seo, K. Development and Characteristics of Aerated Alkali-Activated Slag Cement Mixed with Zinc Powder. *Materials* **2021**, *14*, 6293. [[CrossRef](#)] [[PubMed](#)]

Disclaimer/Publisher’s Note: The statements, opinions and data contained in all publications are solely those of the individual author(s) and contributor(s) and not of MDPI and/or the editor(s). MDPI and/or the editor(s) disclaim responsibility for any injury to people or property resulting from any ideas, methods, instructions or products referred to in the content.